Implications of Flow Angle Stabilization on Coherent E–Region Spectra

P. Janhunen

Department of Geophysics, Finnish Meteorological Institute, Helsinki

Received October 29, 1993; revised February 15, 1994; accepted March 22, 1994

Abstract. Recent perpendicular particle simulations of the Farley–Buneman instability show good agreement with the linear dispersion relation: the phase velocity is proportional to the electric field. This is in contrast with the usually quoted nonlinear theory, which states that the phase velocity at any direction does not rise much above the ion acoustic velocity C_s. However, the simulations also produce a flow angle shift in the spatial power spectrum such that the most intense modes have phase velocities close to C_s. Using simple analytical formulae based on these simulations, we synthesize coherent spectra assuming a turbulent microstructure of the scattering volume. In this way, the observed Type 1 characteristics can be reproduced, and also spectra similar to Type 4 can be generated. A new interpretation of the C_s saturation observed in the equatorial electrojet is thus presented, and the difference between equatorial and auroral coherent spectra becomes understandable.

Introduction

Unstable electrostatic waves are generated in the ionospheric E–region if the external electric field in the neutral rest frame is large enough [e.g., *Farley*, 1985]. Initially, the linear dispersion relation

$$\omega = \frac{kV_d \cos\theta}{1+\psi} \tag{1}$$

was used to explain observed characteristics of coherent spectra in the equatorial electrojet. However, it was soon found that the phase velocity $v_{ph} = \omega/k$ is seldom larger than the ion–acoustic velocity C_s, even when equation(1) would predict so *Farley and Balsley,* 1973, *Sudan et al.,* 1973, *Farley,* 1979, *Farley,* 1985, *Fejer and Kelley,* 1980. Many explanations for the C_s saturation puzzle have been put forward; the anomalous collision theory of *Sudan*[1983] is the most widely accepted.

We now turn to auroral electrojet. In the auroral electrojet, the C_s saturation is realized in a weaker sense: spectral peaks close to C_s are most common, but faster type 4 waves are sometimes observed, too *Haldoupis,* 1989, *Haldoupis and*

Schlegel, 1990. Sudan's theory was extended to include ion kinetic effects and applied to the auroral case *Robinson,* 1986, *Robinson and Honary,* 1990, *Robinson,* 1992. When we use the phrase "Sudan's theory" we refer to the theory of type 1 equatorial waves *Sudan,* 1983, not to the theory of type 2 waves presented in the same paper, and when we are presenting alternatives to Sudan's theory we are not in any way criticizing his type 2 theory.

In this paper we develop a formalism which is suited for both equatorial and auroral regions and which is able to address the question of the markedly different spectral characteristic in these two regions. Earlier small–scale simulation results *Janhunen,* 1994 are used as building blocks in a model for coherent scatter spectra from larger scattering volumes.

Flow angle stabilization

Recent 2D particle simulations in the perpendicular plane *Janhunen,* 1994, which were also verified using 3D codes, were unable to reproduce the anomalous collision effects of Sudan's theory or the local C_s saturation. Instead, it was found that the spectral peak followed quite closely the linear dispersion relation, which was also the outcome of the equatorial *in situ* measurements of *Pfaff* et al. [1987]. The simulations predict an asymmetric distribution of spectral density as a function of flow angle θ [*Janhunen,* 1994, figure 12]. Approximately, this distribution is such that the most intense mode has a flow angle θ satisfying

$$\gamma \sim \left(\frac{kV_d\cos\theta}{1+\psi}\right)^2 - (kC_s)^2 = 0 \tag{2}$$

and the sign of θ is defined by $\mathbf{k}\cdot\mathbf{E} < 0$. Thus, the most intense mode has flow angle

$$\theta_0 = -\left|\arccos\left[\frac{C_s}{V_d}(1+\psi)\right]\right|, \tag{3}$$

zero linear growth rate, and its phase velocity is equal to C_s. Based on simulations *Janhunen,* 1994, we assume the following specific model for the spatial power spectrum as a function of flow angle:

$$I(\theta) \sim \exp\left\{-\left|\frac{\theta-\theta_0}{w_1+(w_2-w_1)\Theta(\theta-\theta_0)}\right|^{3/2}\right\} \tag{4}$$

where $\Theta(x)$ is the Heaviside unit step function, $w_1 = 10^\circ$, $w_2 = \max(w_1, 0.4\,|\theta_0|)$ and θ_0 is given by equation(3). The model is a Gaussian–like distribution with peak position θ_0 and with unequal widths on left and right sides (w_1 and w_2, respectively).

Thus, a nonsymmetric flow angle distribution is central to our interpretation of the simulation results. Nonsymmetric flow angle distribution was observed by *Mattin and Jones* [1987], but it is not yet clear whether it is related to flow angle stabilization or not.

In order to synthesize spectra, we also need the turbulence level $< |\Delta n/n| >$ as a function of the electric field. Again based on simulations, we use

$$\left\langle \left| \frac{\Delta n}{n} \right| \right\rangle \sim \frac{x}{1+x^2} \tag{5}$$

where

$$x = \max[0, \frac{V_d}{(1+\psi)C_s} - 1] \tag{6}$$

tells how much the drift velocity is above the Farley–Buneman threshold $V_d^{thr} = (1+\psi)C_s$.

The essential feature of Eq. (5) is that it produces a steeply rising turbulence level as the threshold is exceeded. The turbulence level has a maximum at $x = 1$ and for $x > 1$ it is weakly decreasing. The decreasing at very large drifts is mainly based on simulations by *Schlegel* [private communication, 1993]. The conclusions of the present paper do not, however, depend on the decreasing since the effect is weak and that large drifts are rare. The steep rising is in agreement with experimental results [e.g., *Nielsen et al.,* 1988].

We also use a dependency of T_e and thus C_s on E based on *Janhunen* [1994]. The details of this are unimportant, it suffices to say that C_s will be about 1.6 times higher for $E = 100$ mV/m than for $E = 0$.

Spectrum synthesization

In this section we use simple numerical methods to visualize the flow angle stabilization. We assume that the measured coherent spectrum, originating from a certain scattering volume, is a superposition of n_p primitive spectra. A primitive spectrum is a narrow (standard deviation 20 m/s) Gaussian peak with mean Doppler shift given by (1). The region of space from which a primitive spectrum originates is called a primitive volume. The scattering from the primitive volumes is described by equations (1) through (6) above. The intensity of the primitive spectrum is given by the product of (4), (5), and the ambient electron density N. To compute a primitive spectrum contribution, we need the ambient electric field E, the flow angle θ, and the electron density N. Notice that we use the symbol n for the microscopic electron density, and the symbol $N = \langle n \rangle$ for the electron density averaged over the primitive volume (N is in general different for different primitive volumes). We use the following assumptions about the statistical nature of the plasma.

1. The large–scale (10 m – 10 km) electron density N obeys a power law turbulence spectrum. Specifically, $N = N_0 \exp(\langle |\Delta N/N_0| \rangle\, f)$ where f obeys power law spectrum with spectral index -2.5 and is normalized so that the standard deviation of f is unity. In addition, the largest wavelengths were filtered out from f. The variability of N inside scattering volume is characterized by the parameter ΔN.

2. Electric field E and electron density N are anticorrelated: $E = (\langle E \rangle / N) N_0$. In a one–dimensional system, this assumption would be exactly true because of current continuity, but it is qualitatively correct for multidimensional systems, too. Notice that the conductivity is proportional to N.

3. Flow angle fluctuation is proportional to the logarithm of the electron density, $\Delta\theta \sim \log(N/N_0)$. While this model is very crude, it still includes the fact that flow angle fluctuations are generally associated with large–scale electron density variations.

In this way, we can synthesize a coherent backscatter spectrum. Our free parameters are the average electric field $\langle E \rangle$, the mean large–scale electron density fluctuation $\langle |\Delta N/N| \rangle$, and the mean flow angle $\langle \theta \rangle$, as well as the number of primitive spectra n_p. The angular brackets within this paragraph refer to averaging over the scattering volume. Figure 1 shows an example of such a spectrum; we have chosen the parameters to simulate a type 1 spectrum.

We now study how the amount of larger scale gradient drift turbulence $\langle |\Delta N/N| \rangle$ affects the spectra. Laminar electrojet conditions ($\langle |\Delta N/N| \rangle = 0.05$) are realized in Figure 2, where the first moment of the simulated spectrum has been plotted against the average electric field. With small electron–density and electric field fluctuations, equation(1) is a good approximation to the simulated Doppler velocity. Figure 3 displays the same information for a turbulent scattering volume ($\langle |\Delta N/N| \rangle = 0.4$). There is more variability in the mean Doppler velocity, but the overall trend is clear: it tends to follow the ion–acoustic velocity, being slightly larger than C_s. Phase velocity being about 15 % above C_s on the average is in agreement with observations *Haldoupis and Schlegel,* 1990.

In Figure 1, the large–scale electron density fluctuation $\langle |\Delta N/N| \rangle$ is 0.2. Thus Figure 1 represents an intermediate case between laminar and turbulent conditions, and therefore the mean Doppler shift of 549 m/s does not agree with Figure 2.

It might be reasonable to assume that the large–scale fluctuation level of the scattering volume somehow depends on the mean electric field intensity. We experimented with various models of this kind. If, for instance, the fluctuation level is proportional to the mean field, the result will look like Figure 3 except that for small field values, the simulated Doppler velocities will follow equation(1) rather than C_s.

Figure 4 is a scatter plot of the first and second spectral moments, sometimes called a Watermann plot *Watermann,* 1989. Each point represents one "event" (simulated coherent spectrum measurement) with definite parameters $\langle E \rangle$, $\langle |\Delta N/N| \rangle$, $\langle \theta \rangle$. Each event is composed of $n_p = 20$ primitive spectra as explained above. We have generated a statistical set of 1000 events for this plot. The electric field and fluctuation level parameters obey exponential distributions, whereas $\langle \theta \rangle$ is uniformly distributed. Notice that these distributions are of "second order", since each event is already a superposition of many primitive spectra. Too

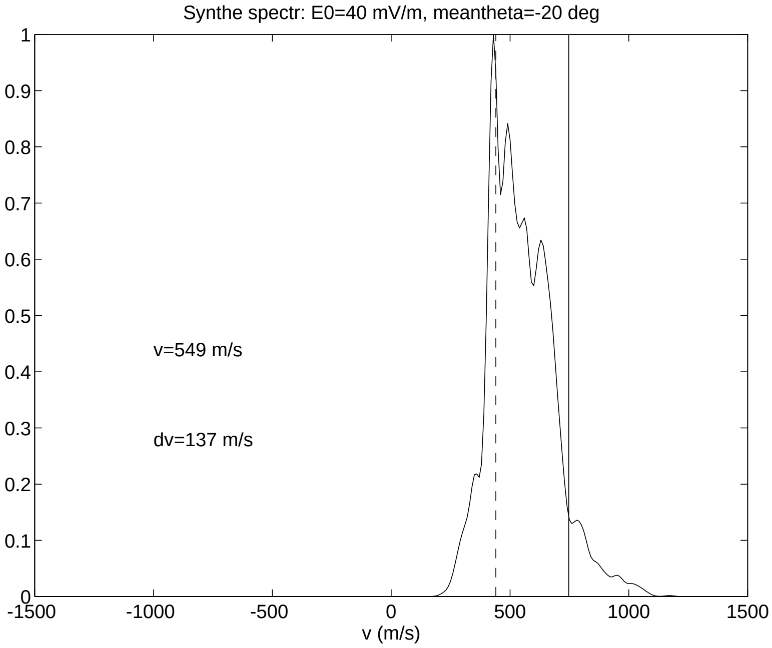

Figure 1. Example "type 1" simulated spectrum. Mean electric field is 40 mV/m, mean flow angle is -20°, and large–scale turbulence level is moderate. The dashed line denotes ion–acoustic velocity C_s, the solid line is the result from equation (1). The exact positions of the individual protuberances depend on the random numbers used in the synthesization procedure.

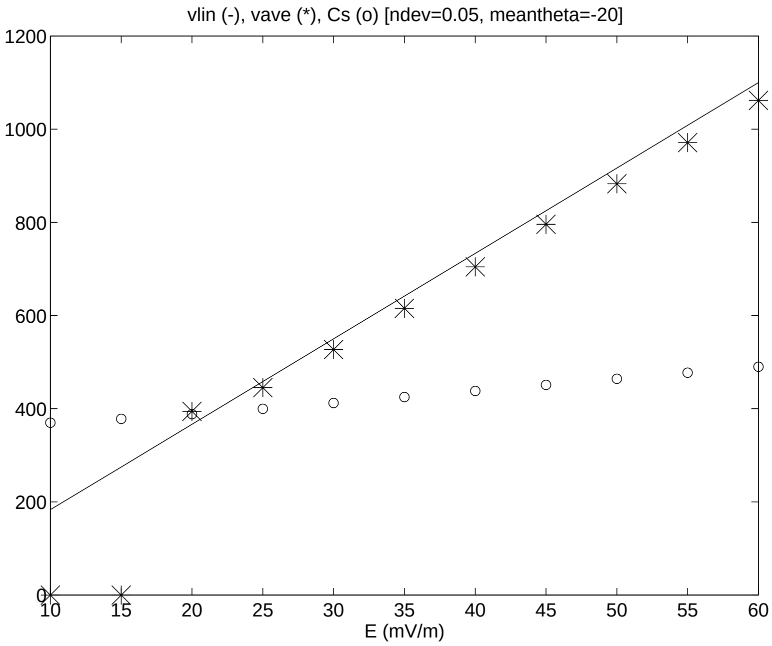

Figure 2. Simulated first moment of Doppler spectrum (stars), ion–acoustic velocity (open circles), and equation (1) (solid line) versus mean electric field. Mean flow angle is -20°, and the scattering volume is assumed to be in a nearly laminar state. Zero Doppler velocity for small electric fields means the absence of coherent echoes.

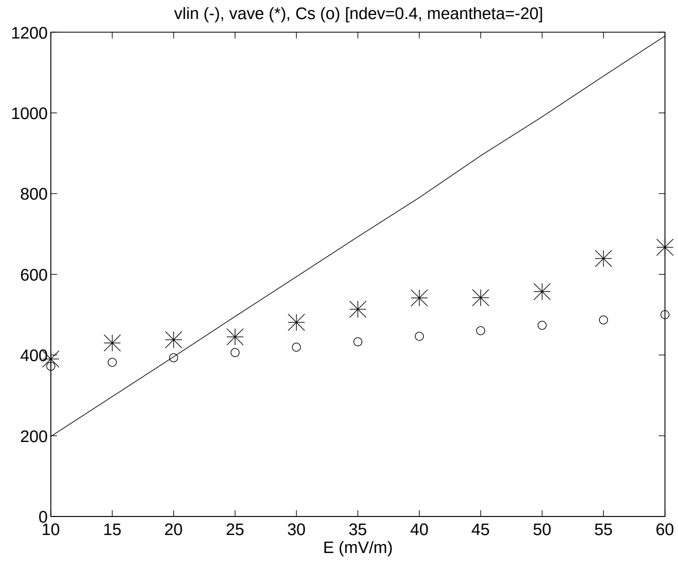

Figure 3. The same as Fig. 2, but for turbulent scattering volume. The first two points (for 10 and 15 mV/m electric field) are somewhat unreliable because the echo strength is small.

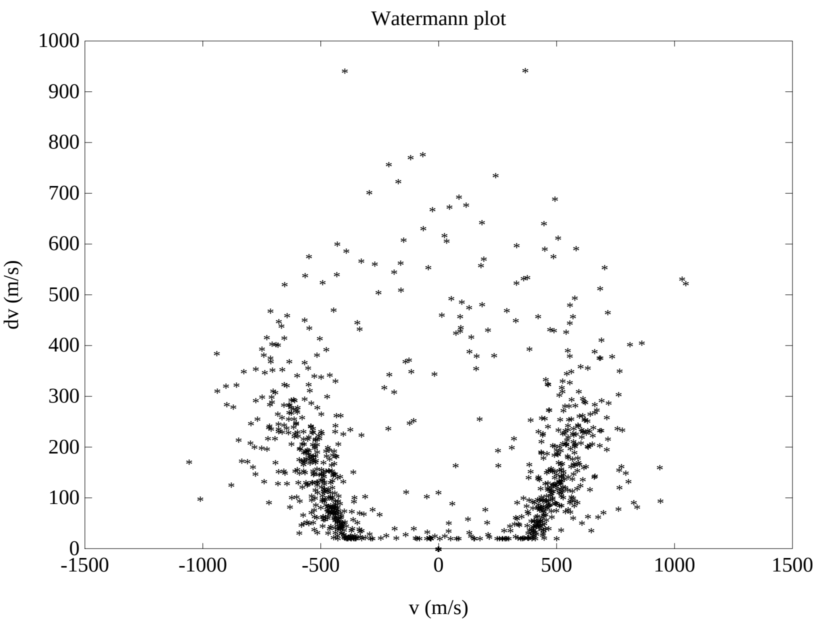

Figure 4. A simulated Watermann plot for the auroral electrojet. The majority of echoes have velocity close to C_s (about 450 m/s), but there are also points with large Doppler velocities (type 4).

weak echoes were not included in the plot. The preference for phase velocities close to C_s, about 450 m/s, is clearly visible. Varying the various parameters does not qualitatively change this result. The second moment is bounded from below since we have assumed a finite, constant width for primitive spectra.

In Figure 4 there is clearly a small linear correlation between first and second moments near the ion–acoustic velocity. The correlation would become more pronounced if the number n_p of primitive spectra in scattering volume was increased. The reason for this is that for large electric fields and large n_p, the spectrum is a superposition of many primitive peaks, each of which has slightly different Doppler shift because the electric field and flow angle vary. Thus the spectral width increases as a function of the electric field. However, if n_p is small (less than 20, say), then the correlation is less clear since many spectra anyway have only one dominant primitive peak.

The choice of n_p deserves a little discussion. In principle one should estimates how many primitive volumes there are in a scattering volume, and use this number as n_p. The scattering volume is typically several kilometers or tens of kilometers in size, whereas the primitive volume may be only a few radar wavelengths across. Our value $n_p = 20$ is thus very small compared to these numbers. Indeed, using an artifically small n_p is just a way to introduce some more 'randomness' in the large–scale electron density and to make the spectra more spiky. A more careful way of accomplishing this would be to use a large n_p and a more complicated model for N, perhaps containing modeled auroral arcs. This approach would require much more computing time, however, and the present method is well suited for our purposes in this paper.

In Figure 5 we have plotted nine synthesized spectra. The corresponding parameters $\langle E \rangle$, $\langle |\Delta N/N| \rangle$, and $\langle \theta \rangle$ are listed in Table 1. In this section we will use the term "turbulence level" to refer to the large–scale turbulence level $\langle |\Delta N/N| \rangle$. Note that entries in Table 1 are in the same order as in Figure 5. It is stressed that Figure 5 is an example only, there is great variability in the synthesized spectra and no statistical conclusions should be drawn from these data.

The first column of Figure 5 contains type 3 spectra. Electric field is modest in all 3 cases, and the turbulence level is small. The mean flow angle is -70° in all cases. Parameters vary slightly in these cases, but the spectrum remains basically the same.

Type 1 spectra are presented in the second column of Figure 5. The electric field and turbulence level increase from top to bottom. The spectra with larger turbulence levels are wider and have multiple peaks, but in all cases the first moment remains close to C_s. Notice that the turbulence level in the second column is overall greater than in the other columns.

The third column of Figure 5 simulates type 4 spectra. The topmost spectrum is very narrow, an electric field of 50 mV/m, and small turbulence level. The mean flow angle is zero in all 3 cases. The electric field and turbulence level increase from top to bottom, and the spectra become wider, as for type 1.

The idea of using spatially averaged primitive spectra to explain the observed spectral features is not new by itself, for example *Uspensky*[1985] and *Kustov and Haldoupis*[1992] used averaging over altitude in their spectrum synthesization. The electrojet microstructure with anticorrelated electron density and electric field have also been studied before *Uspensky et al.,* 1989. The principal difference between the present paper and the previous works is in the use of an asymmetric flow angle distribution, which is based on simulations.

The present method to synthesize spectra is still more a method of visualization than a rigorous statistical estimation. To improve it, the aspect angle dependence of the spatial power spectrum should be estimated and modeled, using 3D simulations or phenomenological knowledge. Also the effect of a zeroth order electron density gradient on the primitive spectrum width should be somehow estimated and taken into account.

It has been verified that the basic results of this paper do not depend on the details of the synthesization procedure (assumptions 1 through 3 above). By making different assumptions on e.g. the flow angle fluctuation dependency on electron density, the resulting spectra would be different, but the basic trends would not be affected.

Interpretation

In this section we discuss how the difference of equatorial and auroral spectra can be understood in terms of flow angle stabilization. The amount of large–scale turbulence is the key factor. If the electrojet were fully laminar, the resulting spectral peak would be given by equation(1) (cf. Fig. 2). If, on the other hand, the electrojet is turbulent and the electric field direction fluctuates a lot within the scattering volume, some of the primitive volumes will have flow angles such that the phase velocities are near C_s. Since waves with phase velocity close to C_s are the most intense, the radar will see mainly phase velocity C_s (cf. Fig. 3), and this is interpreted as C_s saturation. This is especially true if the mean flow angle is close to θ_0.

In the equatorial electrojet there is often a lot of gradient drift turbulence *Farley and Balsley,* 1973, because there is typically a 6 km scale length electron density gradient perpendicular to the magnetic field. Thus the flow direction and magnitude fluctuates, and the radar interprets this as phase speed saturation to C_s.

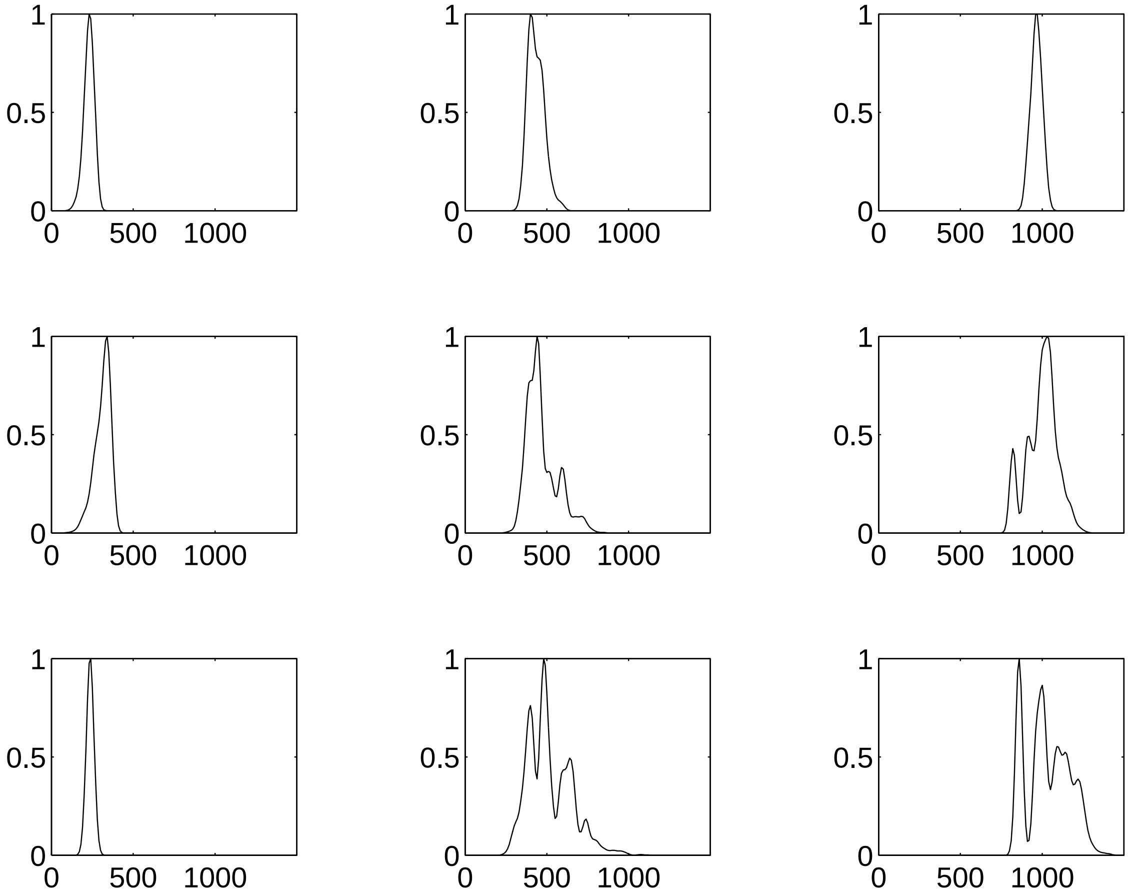

Figure 5. Synthesized self–normalized Doppler spectra for type 3 (leftmost column), type 1 (middle column), and type 4 (rightmost column). Parameters are listed in Table 1. The horizontal axis is the Doppler velocity in m/s, starting from zero. As in Figure 1, the individual spikes in multi–peaked spectra depend on random numbers.

Table 1. Parameters ($\langle E\rangle$, $\langle|\Delta N/N|\rangle$, $\langle\theta\rangle$) for Figure 5. $\langle E\rangle$ is in mV/m, $\langle\theta\rangle$ is in degree.

	Col 1	Col 2	Col 3
Row 1	(25, 0.05, −70)	(25, 0.1, −20)	(50, 0.03, 0)
Row 2	(30, 0.075,−70)	(30, 0.2, −20)	(55, 0.08, 0)
Row 3	(35, 0.01, −70)	(35, 0.3, −20)	(60, 0.1, 0)

In the auroral zone there is no significant permanent perpendicular electron density gradient. However, at times the electron precipitation and other magnetospheric forcing will create large but localized perpendicular gradients. At auroral arcs, the scale length may be of the order of a few hundred meters. Thus both laminar and very turbulent conditions occur, and the flow angle stabilization scenario predicts varying Doppler velocities: most often near C_s (type 1), but occasionally larger, too (type 4). Type 2 spectra are not explicitly present in the formulation since we have not considered gradient drift instability when computing the primitive spectral width.

Although we have here produced large Doppler velocities directly, the "traditional" explanation of type 4 *Fejer et al.,* 1986, *Farley and Providakes,* 1989, involving anomalously high electron temperatures, is also compatible with the flow angle stabilization approach. In fact, there may be two kinds of type 4 peaks: echoes from a turbulent scattering volume with very high electron temperature and electric field, or a laminar region with flow angle close to 0 mod π and with modest electron temperature and electric field. Intermediate cases may also exist. In the first case we would also expect relatively weaker echoes with very high (up to 2000 m/s) Doppler velocities. Such velocities have sometimes been reported *Greenwald and Ecklund,* 1975.

Our scheme also produces small Doppler speeds (Figure 4) characteristic to type 3 spectra *Haldoupis et al.,* 1992, but whether or not these are frequent and strong enough to explain type 3 is still unclear. It has been reported *Haldoupis et al.,* 1993 that there are gaps between type 3, 1, and 4 peaks. The flow angle stabilization does not provide any new clue for this phenomenon.

Conclusions

We have demonstrated that many observational characteristics of both equatorial and auroral coherent spectra can be understood using the flow angle stabilization approach instead of the usual anomalous collision theory (Sudan's theory), which beautifully explained the equatorial electrojet C_s saturation phenomenon. The concept of flow angle stabilization, which is based on particle simulations *Janhunen,* 1994, means that the strongest waves have flow angle that makes their phase velocity close to C_s. In the present paper we extended the previous work by considering an ensemble of small volumes, each obeying flow angle stabilization. The large–scale (more than 10 m) turbulence level of the electrojet scattering volume determines the properties of the spectra. If the electrojet is laminar (i.e., has little gradient drift turbulence), the spectra will obey linear theory, if it is turbulent, they will display C_s saturation.

The remaining task is now to test the consistency and relevance of flow angle stabilization. To this end, more large–scale computer simulations should be performed to test the aspect angle and flow angle effects together and to test the influence of electron density gradients on the Farley–Buneman waves. Observational testing should include combined coherent/incoherent scatter observations of the same volume, using at least two coherent radars, as well as statistical examination of the spectra to more accurately determine the geophysical conditions associated with each spectral type. Pioneering statistical studies [*e.g., André,* 1983] have used only small data sets.

If it turns out at the end that flow angle stabilization is correct and relevant, as both 2D and 3D simulations suggest, then this may open up new opportunities for deducing the geophysical conditions of the scattering volume from spectral information. It should in principle be possible to use formulas like those in this paper in a statistical inversion theoretical approach to determine the properties of the scattering volume from the spectral data. The success of such an approach is, however, dependent on how accurately the spatial power spectrum can be determined from the simulations, and there is clearly much to improve in this respect.

Acknowledgments. The author thanks Asko Huuskonen for reading the manuscript and making a number of useful comments. The simulations on which this work is based were carried out on a Cray X–MP located at Centre of Scientific Computing, Espoo, Finland.

References

André, D., The dependence of the relative backscatter cross section of 1-m density fluctuations in the auroral electrojet on the angle between electron drift and radar wave vector, *J. Geophys. Res., 88,* 8043–8049, 1983.

Farley, D.T., and Balsley, B.B., Instabilities in the equatorial electrojet, *J. Geophys. Res., 78,* 227–239, 1973.

Farley, D.T., The ionospheric plasma, in *Solar System Plasma Physics,* edited by C.F. Kennel, L.J. Lanzerotti, and E.N. Parker, chap. III-1-7, North–Holland, Amsterdam, 1979.

Farley, D.T., Theory of equatorial electrojet plasma waves: new developments and current status, *J. Atmos. Terr. Phys., 47,* 729–744, 1985.

Farley, D.T., and Providakes, J., The variation with T_e and T_i of the velocity of unstable ionospheric two–stream waves, *J. Geophys. Res., 94,* 15415–15420, 1989.

Fejer, B., and Kelley, M.C., Ionospheric irregularities, *Rev. Geophys. Space Phys.,* 18 401–454, 1980.

Fejer, B.G., Providakes, J., Farley, D.T., and Swartz, W.E., Auroral E region plasma waves and elevated electron temperatures, *J. Geophys. Res., 91,* 13583–13592, 1986.

Greenwald, R.A., and Ecklund, W.L., A new look at radar auroral motions, *J. Geophys. Res., 80,* 3642–3648, 1975.

Haldoupis, C., A review on radio studies of auroral E–region ionospheric irregularities, *Ann. Geophys., 7,* 329–258, 1989.

Haldoupis, C., and Schlegel, K., Direct comparison of 1-m irregularity phase velocities and ion acoustic speeds in he auroral E–region ionosphere, *J. Geophys. Res., 95,* 18989–19000, 1990.

Haldoupis, C., Schlegel, K., and Nielsen, E., On type 3 auroral VHF coherent radar backscatter, *J. Geophys. Res., 97,* 4109–4120, 1992.

Haldoupis, C., Koehler, J.A., Sofko, G.J., Danskin, D.W., McKibben, M.J., and André, D., Preferential phase velocities for type 4 irregularities in the auroral E region plasma, *J. Geophys. Res., 98,* 6173–6179, 1993.

Janhunen, P., Perpendicular particle simulation of the E–region Farley–Buneman instability, *J. Geophys. Res., in,* press, 1994.

Kustov, A.V., and Haldoupis, C., Irregularity drift velocity estimates in radar auroral backscatter, *J. Atmos. Terr. Phys., 54,* 415–423, 1992.

Mattin, N., and Jones, T.B., Propagation angle dependence of radar auroral E–region irregularities, *J. Atmos. Terr. Phys., 49,* 115–121, 1987.

Nielsen, E., Uspensky, M., Kustov, A., Huuskonen, A., and Kangas, J., On the dependence of the Farley–Buneman turbulence level on ionospheric electric field, *J. Atmos. Terr. Phys., 50,* 601–605, 1988.

Pfaff, R.F., Kelley, M.C., Kudeki, E., Fejer, B.G., and Baker, K.D., Electric field and plasma density measurements in the strongly driven daytime equatorial electrojet, *J. Geophys. Res., 92,* 13597–13612, 1987.

Robinson, T.R., Towards a self–consistent non–linear theory of radar auroral backscatter, *J. Atmos. Terr. Phys., 48,* 417–422, 1986.

Robinson, T.R., and Honary, F., A resonance broadening kinetic theory of the modified two–stream instability: implications for radar auroral backscatter experiments, *J. Geophys. Res., 95,* 1073–1085, 1990.

Robinson, T.R., The effects of the resonance broadening of Farley–Buneman waves on electron dynamics and heating in the auroral E–region, *J. Atmos. Terr. Phys., 54,* 749–757, 1992.

Sudan, R.N., Akinrimisi, J., Farley, D.T., Generation of small–scale irregularities in he equatorial electrojet, *J. Geophys. Res., 78,* 240–248, 1973.

Sudan, R.N., Unified theory of type I and type II irregularities in the equatorial electrojet, *J. Geophys. Res., 88,* 4853–4860, 1983.

Uspensky, M.V., On the altitudinal profile of auroral radar backscatter, *Radio Sci., 20,* 735–739, 1985.

Uspensky, M.V., Kustov, A.V., Williams, P.J.S., Huuskonen, A., Kangas, J., and Nielsen, E., Effect of unresolved electrojet microstructure on measurements of irregularity drift velocity in auroral radar backscatter, *Adv. Space Res.,* 9, 5119–5122, 1989.

Watermann, J., McDiarmid, D., McNamara, A.G., Koehler, J.A., and Sofko, G.J., Are type III radio aurorae directly excited by electrostatic ion cyclotron waves?, *J. Geophys. Res., 94,* 13479–13488, 1989.

This manuscript was prepared with the AGU LaTeX macros v3.0.